Research Article
Sciences of Phytochemistry

Unraveling the Anti-HCV Mechanism of the Ethyl Acetate Fraction of *Vitex cofassus* via Integrated Network Pharmacology and Molecular Dynamics Simulation

Puput Widarini, Sri Wahyuli, Ruslin Ruslin, Setyanto Tri Wahyudi, Muhammad Arba

[The author informations are in the declarations section. This article is published by ETFLIN in Sciences of Phytochemistry, Volume 5, Issue 2, 2026, Page 346-358. DOI: 10.58920/sciphy0502687]

Received
11 May 2026

Revised
05 July 2026

Accepted
12 September 2026

Published
07 November 2026

Editor
Sanchaita Rajkhowa

Keywords: Hepatitis C, LC-HRMS, molecular docking, network pharmacology.

CC BY 4.0

AUTHOR (2026)

Abstract: To address the growing health burden posed by the hepatitis C virus (HCV), the present study employed computational approach to predict the medicinal properties of *Vitex cofassus*. Liquid chromatography-high resolution mass spectrometry (LC-HRMS) analysis of its ethyl acetate leaf fraction identified 37 drug-like compounds. Network pharmacology predicted 201 biological targets, with key proteins such as STAT3, IL6, SRC, AKT1, EGFR, HSP90AA1, and TNF-α being central to the proposed mechanism of action. Functional enrichment analyses pointed to involvement in chemical response, intracellular signaling, stress, and regulated cell death, with molecular functions linked to kinase activity and ATP binding. KEGG analysis further associates targets with key pathways in cancer, viral infection, and metabolic disease. Picrocrocin and flavonoids such as isorhamnetin and apigenin were predicted as potential inhibitors of HCV-related proteins (STAT3 and SRC, respectively). While these *in silico* findings provide a rational basis for further investigation, the present findings remain predictive and require experimental validation to confirm actual anti-HCV efficacy.

Introduction

Hepatitis C virus (HCV) infection remains a formidable global health challenge, affecting millions worldwide and representing a leading cause of chronic liver disease, cirrhosis, and hepatocellular carcinoma. The advent of direct-acting antivirals (DAAs) has undoubtedly revolutionized the treatment of hepatitis C, achieving remarkable cure rates, though these are not infallible. The threat of drug resistance, the high cost of therapy that limits access in resource-poor settings, and the potential for late-stage diagnosis where advanced liver damage diminishes treatment efficacy underscore the persistent need for novel therapeutic strategies. Consequently, the scientific pursuit for alternative, cost-effective, and broad-spectrum anti-HCV agents is more critical than ever.

A significant proportion of the world's population (approximately 80%) utilizes traditional and complementary medicine (T&CM), frequently in conjunction with conventional healthcare services. Acknowledging this, the World Health Organization (WHO) has advocated for the integration of T&CM into national healthcare frameworks to guarantee standardized quality —an advocacy reinforced by substantial ethnobotanical data records pertaining to plants utilized in the treatment of infections (1). The *Vitex* genus, which is part of the Lamiaceae family, is a notable group within these records and valued for its diversity of bioactive phytochemicals, such as flavonoids, terpenoids, and lignans (2). These compounds are associated with a broad range of pharmacological properties, including antimicrobial, anticancer, and hepatoprotective effects (3 – 12). Extracts from several *Vitex* species have been observed to show direct activity against diverse pathogens (13). Of particular relevance to antiviral drug discovery, *Vitex negundo* extracts have shown significant activity against SARS-CoV-2, with demonstrated inhibition of viral replication and suppression of RNA-dependent RNA polymerase (RdRp) activity in a dose-dependent manner (14). Furthermore, extracts of *Vitex doniana* have exhibited anti-HIV-1 activity with an IC_{50} of 25 µg/mL (15, 16), suggesting that bioactive constituents within this genus may target viral replication mechanisms across different viral families. In addition, *V. negundo* ethanolic extracts have demonstrated hepatoprotective effects in thioacetamide-induced liver cirrhosis models, attenuating oxidative stress through normalization of endogenous antioxidant (17). Importantly

for HCV-specific activity, flavonoids including apigenin and luteolin, which are found in various *Vitex* species, have been demonstrated to inhibit HCV replication (18). These findings establish a plausible mechanistic link between *Vitex*-derived flavonoids and HCV inhibition.

Despite the extensive pharmacological characterization of other *Vitex* species, research specifically addressing *Vitex cofassus* remains limited. Phytochemical investigations have identified clerodane diterpenes, including 16-hydroxy-pentandralactone and acuminolide, from *V. cofassus* leaves, which demonstrated potent antiproliferative activity against human tumor cell lines (IC_{50} values of 5.4–11.4 μM) and inhibition of VEGF-stimulated endothelial cell proliferation, suggesting anti-angiogenic potential (3). Flavonoid constituents have also been detected in *V. cofassus* extracts, consistent with the phytochemical profiles of other bioactive *Vitex* species. However, these studies have not explored antiviral activity, and no published data exist on the anti-HCV potential of *V. cofassus* or its isolated compounds. The specific molecular targets through which *V. cofassus* compounds might exert antiviral effects, the predicted binding interactions with HCV proteins, and the broader polypharmacological network modulating host-virus interactions remain entirely unknown.

To address this gap, the present study employs a computational approach integrating LC-HRMS-based phytochemical profiling, network pharmacology, molecular docking, and molecular dynamics simulation to predict the anti-HCV potential of *V. cofassus* ethyl acetate leaf fraction. This study provides the first *in silico* evidence for the mechanism of action of ethyl acetate leaf fraction of *V. cofassus* against HCV and establishes a theoretical foundation for subsequent experimental validation.

Methodology

Preparation and Chemical Characterization of the Plant Fraction

Fresh leaves of *V. cofassus* were collected in June 2024 from the Gantara Forest Management Unit in Southeast Sulawesi Province, Indonesia. The species was authenticated at the Universitas Halu Oleo Pharmacy Laboratory (voucher specimen FF-UHO-062). The leaves were processed by a method that involved washing, thin-slicing, and air-drying to produce crude drug (*simplisia*). A methanolic extract of the crude was then obtained through a process of maceration, followed by fractionation by ethyl acetate solvent.

Chemical profiling was performed by means of liquid chromatography–high resolution mass spectrometry (LC–HRMS) using a Thermo Scientific™ Vanquish™ UHPLC system coupled to a Q Exactive™ hybrid quadrupole-Orbitrap™ mass spectrometer. Sample of 5-10 mg was dissolved in 1 mL solvent (water, methanol, acetonitrile). Mobile phase consisted of solvent A, 0.1% (v/v) formic acid in water (MS-grade), and solvent B, 0.1% (v/v) formic acid in acetonitrile (MS-grade). It was used as gradient solvent for eluting the sample with flow rate 0.3 mL/min, starting with injection of 5% of solvent B and was gradually increased to 90% in 16 min, maintained for 4 min, and the system was returned to the initial conditions in 25 min. The separation of the compounds was carried out on an Accucore™ Phenyl-Hexyl column (100 mm × 2.1 mm, 2.6 μm). Column temperature was maintained at 40 °C with injection volume 3 μL. The m/z range was 66.7-1000 m/z with resolution 70,000 (full MS) and 17,500 (dd-MS2). HRMS mode was maintained on MS/dd-MS2 acquisition mode with positive ionization with the help of XCalibur 4.4 software. The analysis was performed once. The data was processed with the help of *Compound Discoverer™3.2* software and compound identification was performed based on database of mzCloud™ and Chemspider™. The constituent identification process was performed in accordance with established protocols (19), with a mass error tolerance of approximately 5 ppm, a confidence score threshold of greater than 80%, and database searches against ChemSpider and mzCloud. Based on the Metabolomics Standards Initiative (MSI) guidelines, the identified compounds were reported at Level 2 (putatively annotated compounds) (20). A detailed list of the identified compounds is provided in Table S1.

Evaluation of Drug-likeness and Target Prediction

The drug-like properties of the identified compounds were assessed using the SwissADME web tool (21). This assessment was conducted based on Lipinski's Rule of Five, which establishes thresholds set for molecular weight (≤ 500 Da), hydrogen bond donors (≤ 5), hydrogen bond acceptors (≤ 10), and lipophilicity (log P ≤ 5). For subsequent analysis, only compounds that satisfied stringent criteria were selected. These criteria included a drug-likeness score of greater than 0.18, a bioavailability score of greater than 0.55, and high gastrointestinal absorption. Compounds that violated more than one of Lipinski's rules or failed the additional filters were systematically excluded.

Prediction of Protein Targets

The potential protein targets of the bioactive compounds were forecasted using the SwissTargetPrediction and Similarity Ensemble Approach (SEA) databases (22, 23). In parallel, a compendium of hepatitis C-associated genes was compiled from the OMIM and GeneCards databases, from which only top 500 targets of GeneCards were selected for further investigation sorted by ''relevance score" in descending order (24–26). The intersection between the predicted targets of the plant compounds and the hepatitis C-related genes was identified and graphically represented using a Venn diagram (https://bioinformatics.psb.ugent.be/webtools/Venn).

Network Construction and Functional Enrichment Analysis

A protein-protein interaction (PPI) network for the common targets was constructed using the STRING database, with the search confined to *Homo sapiens* and a high confidence interaction score of 0.700. The resulting network was imported into Cytoscape (v. 3.10.2) for visualization and topological analysis (27). In order to gain insight into the biological significance of the overlapping targets, Gene Ontology (GO) enrichment analysis (covering biological processes, cellular components, and molecular functions) and Kyoto Encyclopedia of Genes and Genomes (KEGG) pathway analysis were conducted using the Metascape and shinyGO platforms (28–30).

A nominal P-value threshold of < 0.05 was applied as

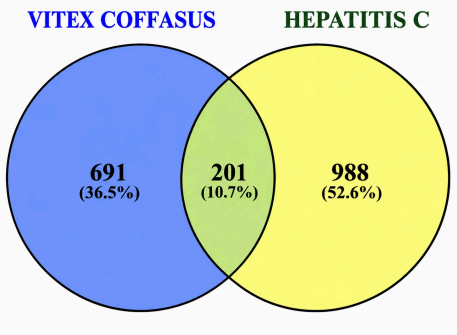


Figure 1. A Venn diagram illustrating that 201 genes were targeted by both hepatitis C and *V. cofassus* compounds, while total 1,189 genes were associated by hepatitis C and 892 genes were associated by *V. cofassus* compounds.

the initial filtering criterion to identify potentially enriched terms (31). To correct for multiple hypothesis testing across hundreds of simultaneously evaluated GO terms and KEGG pathways, the False Discovery Rate (FDR) was calculated using the Benjamini-Hochberg method (32). Only terms with an FDR-adjusted Q-value < 0.05 were considered statistically significant and retained for biological interpretation. Enrichment significance was visualized using-log10(adjusted P-value), where values exceeding 1.3 (corresponding to $P < 0.05$) and 2.0 (corresponding to FDR < 0.01) indicate increasing statistical confidence.

Molecular Docking Simulations

In order to explore binding affinities and modes of interaction, molecular docking was performed between the selected compounds and three key hepatitis C-related protein targets: STAT3, IL6, and SRC. The three-dimensional structures of the proteins were retrieved from the Protein Data Bank (PDB). The two-dimensional ligand structures were converted into three-dimensional formats and energetically minimized using the LigPrep module within the Maestro Schrödinger suite (v. 11.1.012), applying the OPLS_2005 force field (33–35). Proteins were prepared according to standard protocols, and docking grids were generated centered on the binding sites of native co-crystallized ligands. In the present study, a rigid-receptor docking approach was employed, using the crystal structures of the target proteins as the receptor model.

To validate the reliability of our docking protocol, we first performed a redocking experiment using the co-crystallized ligands extracted from the target protein structures (STAT3, PDB ID:6NJS, IL6, PDB ID:1N26, SRC,

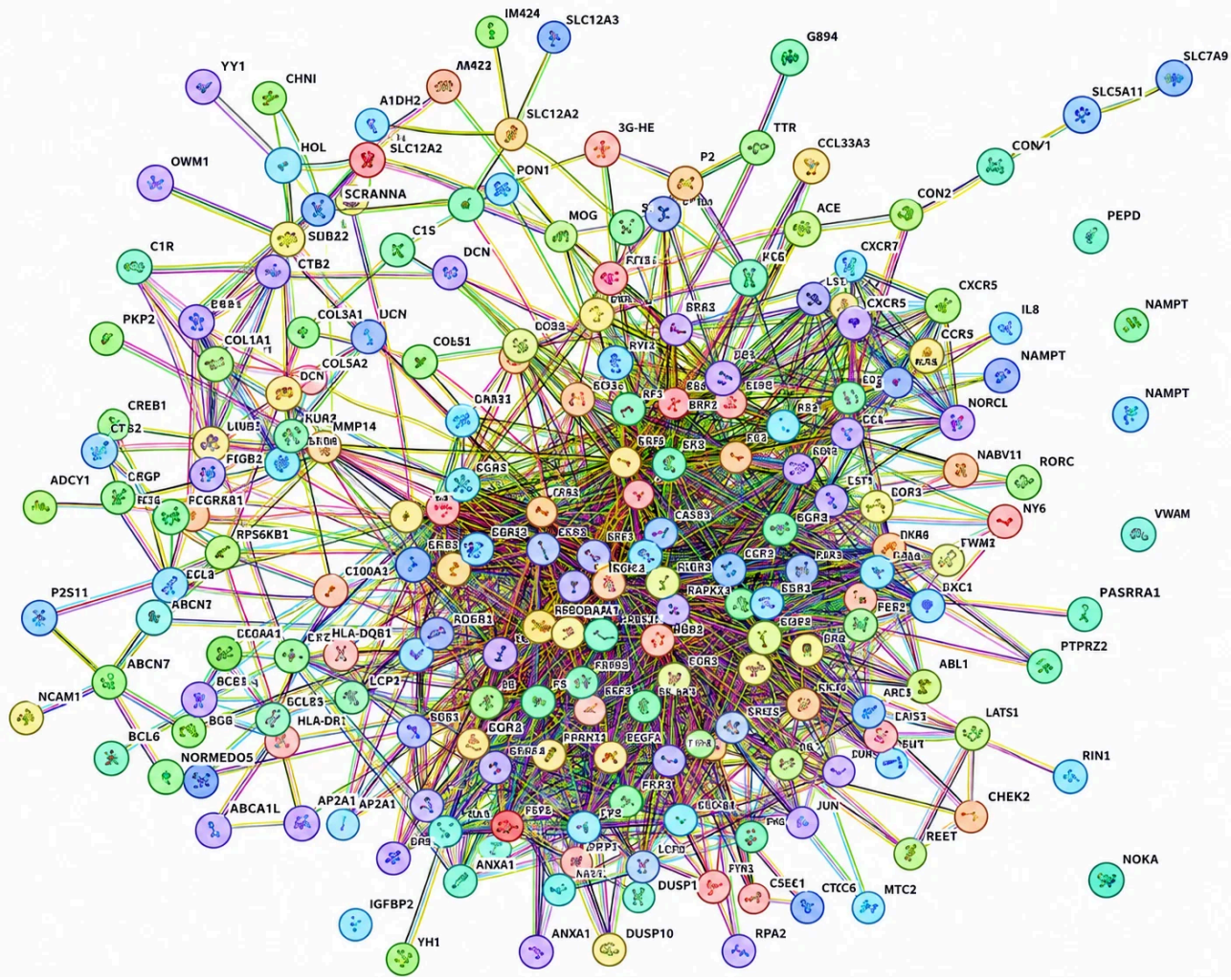


Figure 2. The protein–protein interaction (PPI) network consisting of 201 nodes and 1,448 edges.

Table 1. The 10 most critical hub targets, as identified by their high scores in degree, closeness, and betweenness centrality.

Name	Degree	Closeness	Betweenness
STAT3	71	0.527	0.057
IL6	66	0.527	0.088
SRC	66	0.527	0.064
AKT1	66	0.533	0.066
EGFR	65	0.530	0.071
CTNNB1	59	0.517	0.045
HSP90AA1	58	0.510	0.061
TNF	56	0.516	0.059
MAPK1	49	0.490	0.030
JUN	49	0.506	0.019

PDB ID:2SRC). The ligand was re-docked into the binding site using software parameters as employed for the virtual screening. The root-mean-square deviation (RMSD) between the re-docked pose and the crystallographic conformation was calculated, and an RMSD value ≤ 2.0 Å was considered indicative of successful reproduction of the experimental binding mode.

We acknowledge that docking benchmarking against decoy sets or cross-validation with known inhibitors was not performed in this study. Instead, our validation focused on the internal consistency of the docking protocol through redocking, which is the most direct test of whether the docking protocol used correctly model the known binding geometry. The selection of final docking poses for each compound performed by visual inspection using Maestro, with selection based on the formation of essential interactions with key active-site residues and consistency with the binding mode of the co-crystallized reference ligand.

Molecular Dynamics Simulations

The stability of the top protein-ligand complexes identified from docking was evaluated through molecular dynamics (MD) simulations conducted over a 200 ns timeframe for each target (STAT3 and SRC). Each complex was solvated in an orthorhombic box of SPC water molecules with a 10 Å buffer zone and neutralized with 0.15 M NaCl. Systems were prepared using the OPLS3 force field within the Desmond System Builder (Maestro, Linux). The simulations proceeded through a standard protocol of relaxation, energy minimization, and production, as described in established methodologies (36, 37).

Equilibration was confirmed by monitoring temperature, pressure, and potential energy during the

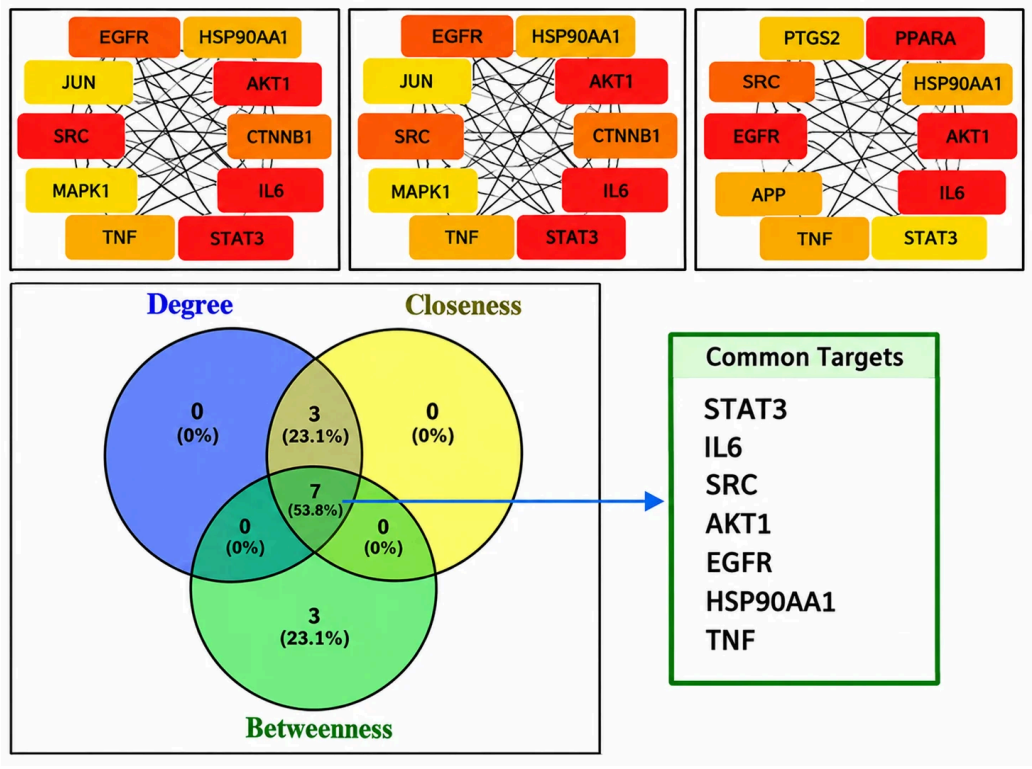


Figure 3. The Venn diagram illustrating that seven proteins—STAT3, IL6, SRC, AKT1, EGFR, HSP90AA1, and TNF-α—were consistently identified as key targets by the three centrality measures, i.e. degree, betweenness, and closeness.

final equilibration phase. For production stability, we monitored the Cα-RMSD and the ligand heavy-atom RMSD. The trajectories were analyzed using the Desmond Simulation Interaction Diagram (SID) tool to calculate root mean square deviation (RMSD), root mean square fluctuation (RMSF), and protein-ligand interaction profiles. System stability was confirmed by monitoring the RMSD of protein Cα atoms, where plateaued values indicated successful equilibration and stable dynamics.

Results

Identification of Bioactive Compounds and Putative Targets

Liquid chromatography–high resolution mass spectrometry (LC–HRMS) analysis of the ethyl acetate fraction of *V. cofassus* leaf led to the identification of a set of 232 bioactive compounds. Subsequent drug-likeness screening filtered this set to 37 compounds that met the criteria for further investigation. The target prediction for these 37 compounds yielded 892 potential human protein targets. Through an analysis of disease-associated databases, after removing duplicates, 1,189 genes related to hepatitis C were compiled originating from 500 genes of Genecards and 882 genes of OMIM. A comparative analysis revealed 201 targets common to both the *V. cofassus* compounds and hepatitis C, which were defined as the key targets for this study (**Figure 1** and **Supplementary Tables 1**–**2**).

Compound-target and Protein-protein Interaction Network Analysis

A compound-target network was constructed to map the interactions between the 37 bioactive compounds and the 201 common targets. Protein–protein interaction (PPI) data for these targets were obtained from the STRING database and visualized in Cytoscape, forming a network of 201 nodes connected by 1,448 edges (**Figure 2**).

A subsequent topological analysis, employing degree centrality as a ranking metric, identified the top 10 hub targets. These targets, along with their closeness and betweenness centrality metrics, are detailed in **Table 1**.

The consensus across three centrality measures—degree, closeness, and betweenness—identified seven proteins (STAT3, IL6, SRC, AKT1, EGFR, HSP90AA1, and TNF-α) as the most critical candidates for therapeutic intervention (**Figure 3**) (38).

Functional Enrichment Analysis of Common Targets

In order to elucidate the potential anti-hepatitis C mechanisms, a functional enrichment analysis of the 201 common targets was performed using Gene Ontology (GO) and Kyoto Encyclopedia of Genes and Genomes (KEGG) databases. The analysis yielded significant enrichment in terms relevant to the disease, revealing 1,000 biological processes (BPs), 249 cellular components (CCs), 683 molecular functions (MFs), and 249 KEGG pathways.

The top biological processes included response to oxygen-containing compound, response to chemical, cellular response to chemical stimulus, cellular response to oxygen-containing compound, intracellular signal transduction, response to stress, cell death, programmed cell death, regulation of programmed cell death, and response to nitrogen compound (**Figure 4A**). Cellular component analysis indicated localization to cell junction, vesicle, membrane raft, membrane microdomain, cell surface, mitochondrion, perinuclear region of cytoplasm, cytoplasmic vesicle, intracellular vesicle, and endoplasmic reticulum (**Figure 4B**). The molecular functions that were predominantly enriched included enzyme binding,

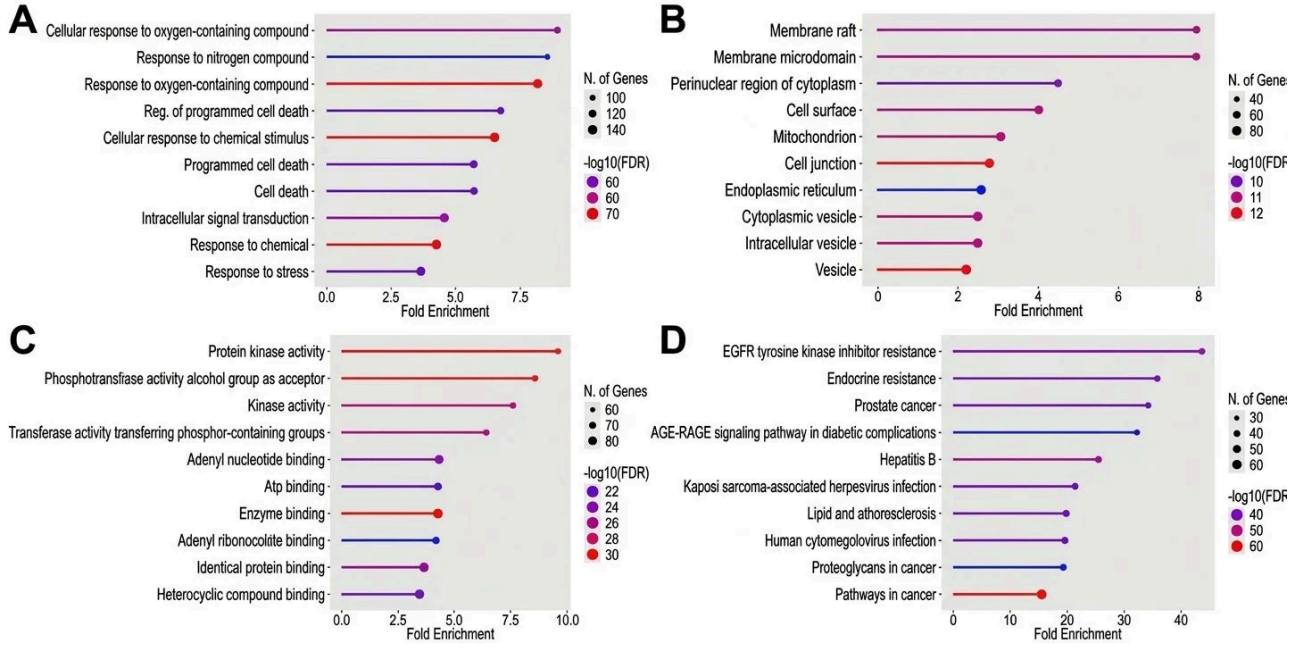


Figure 4. A plot summarizing the bioactive compounds present in the *V. cofassus* leaf ethyl acetate fraction, and depicting their associated Gene Ontology (GO) of biological processes (A), cellular component (B), molecular functions terms (C), and KEGG pathways (D).

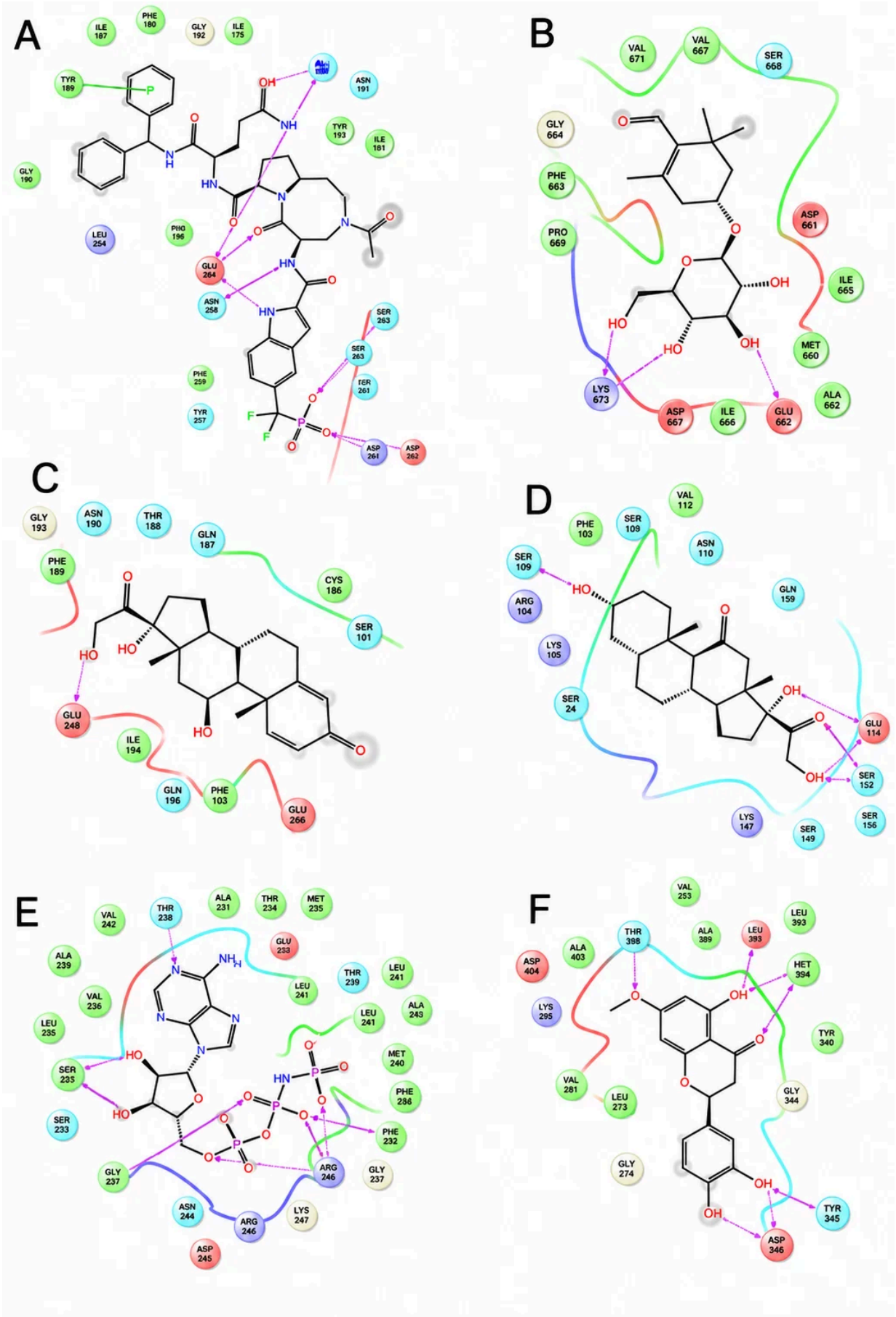


Figure 5. The docked conformation of compounds bound to STAT3, IL6, and SRC. (A–B) Compounds bound to STAT3: (A) KQV and (B) Comp87/Picrocrocin. (C–D) Compounds bound to IL6: (C) Prednisolone and (D) Comp76/Tetrahydrocortisone. (E–F) Compounds bound to SRC: (E) Native ligand (ANP) and (F) Comp4.

Table 2. The binding energy (kcal/mol) of compounds docked to STAT3, IL6, and SRC.

Protein	Binding energy (kcal/mol)		
	STAT3 (PDB ID :6NJS)	**IL6 (PDB ID :1N26)**	**SRC (PDB ID :2SRC)**
Reference compound	**KQV: -9.389**	**Prednisolone: -4.180**	**ANP: -12.562**
Comp4	-	-	-10.943
Comp20/Isorhamnetin	-	-	-9.748
Comp25/4-Oxotretinoin	-	-	-7.142
Comp49	-	-	-9.172
Comp60	-	-	-7.783
Comp72/Apigenin	-	-	-8.663
Comp74/Padmatin	-	-	-10.505
Comp76/Tetrahydrocortisone	-	-4.220	-
Comp83/Lovastatin	-	-	-6.112
Comp87/Picrocrocin	-5.756	-	-
Comp96	-	-	-5.741
Comp133	-	-	-7.774
Comp139/Kaempferol	-	-	-8.475
Comp145/Cortisol	-	-3.931	-
Comp157	-	-3.637	-
Comp163	-	-3.009	-
Comp170/Pinocembrin	-	-	-7.385
Comp193/Drotaverine	-	-	-4.923
Comp214	-	-	-9.209
Comp215/Salvigenin	-	-	-8.624
Comp219/Hydroxyibuprofen	-	-	-5.074
Comp228/Testosterone	-	-2.618	-

phosphotransferase activity with an alcohol group as an acceptor, protein kinase activity, kinase activity, transferase activity transferring phosphorus-containing groups, adenyl nucleotide binding, identical protein binding, adenyl ribonucleotide binding, ATP binding, and heterocyclic compound binding (**Figure 4C**). Of particular significance is the finding that KEGG pathway analysis linked the targets to pathways in cancer, EGFR tyrosine kinase inhibitor resistance, hepatitis B, endocrine resistance, lipid and atherosclerosis, kaposi sarcoma-associated herpesvirus infection, human cytomegalovirus infection, prostate cancer, age-rage signaling pathway in diabetic complications, and proteoglycans in cancer (**Figure 4D**).

Molecular Docking Validation of Key Interactions

Based on the network pharmacology results, STAT3, IL6, and SRC were selected for molecular docking study. Validation of docking protocol was performed by redocking of native ligands. **Figure S1** shows the superimpositions of experimental and docked conformations of native ligand of STAT3 (PDB ID: 6NJS) and SRC (PDB ID: 2SRC) with RMSD 1.8621 Å and 0.9599 Å, respectively, confirming that our docking setup accurately reproduces the native binding modes (RMSD ≤ 2.0 Å). A potential limitation of our docking is the use of a rigid receptor model, which does not fully capture the conformational dynamics of the binding site. Nevertheless, our subsequent molecular dynamics simulation on the top hits indicated that the active site exhibits moderate adaptability, with only a few key residues showing major conformational changes. This suggests that the rigid-docking approach was adequate for initial pose generation, while the MDS results provide a more refined picture over longer timescales.

The results of binding affinity analysis show that Comp87/Picrocrocin, when bound to STAT3, exhibited binding energy of -5.756 kcal/mol, in comparison to the binding energy of -9.389 kcal/mol exhibited by STAT3 when bound to its native ligand (KQV) (see **Figure 5A** and **5B**). Comp87/Picrocrocin formed H-bonds with Glu625 and Lys626, while KQV formed H-bond interactions with Arg609, Ser611, Glu612, Ser613, Ser636, Glu638, and Gln644, and pi-pi interaction with Tyr640. The binding affinities and interactions of the top-scoring compounds are summarized in **Table 2**.

With IL6, five compounds, i.e. Comp76/Tetrahydrocortisone, Comp145/Cortisol, Comp157, Comp163, and Comp228/Testosterone, each bound with binding energies -4.220 kcal/mol, -3.931 kcal/mol, -3.637 kcal/mol, -3.009 kcal/mol, and -2.618 kcal/mol, respectively. Prednisolone formed H-bond with Glu283, while Comp76/Tetrahydrocortisone formed H-bonds with Ser109, Glu114, and Ser152. Comp145/Cortisol (binding energy of -3.931 kcal/mol) formed H-bond with Thr188, Gln190, and Gln196, Comp157 (binding energy of -3.637 kcal/mol) formed Hbonds with Cys102, Gln196. Comp163 (binding energy of -3.009 kcal/mol) formed H-bonds with Lys105 and Gln158, while Comp228/Testosterone (binding energy of -2.618 kcal/mol) formed H-bond with Gln190 (**Figure 5C**, **5D**, and **S2**).

The compounds bound to SRC exhibited a range of binding energy values, from-4.923 kcal/mol (Comp193/Drotaverine) to-10.943 kcal/mol (Comp4), in comparison to the binding energy of the native ligand (ANP) bound to SRC, which was-12.562 kcal/mol. Comp4 formed H-bonds with Asp348, Ser345, Thr338, Met341, and Glu339 (**Figure 5E** and **5F**). Comp20/Isorhamnetin

(binding energy of-9.748 kcal/mol) formed H-bonds Thr338, Asp404, Asn391, Ala390, Leu273, and Met341. Comp25/4-Oxotretinoin (binding energy of-7.142 kcal/mol) formed H-bonds with Cys277, Arg388, and Met341. Comp49 (binding energy of-9.172 kcal/mol) formed H-bonds with Asp404 and Met341. Comp60 (binding energy of-7.783 kcal/mol) formed H-bonds with Ser342 and Thr338. Comp72/Apigenin (binding energy of-8.663 kcal/mol) formed H-bonds with Asp404, Met341, and Leu273. Comp74/Padmatin, with a binding energy of-10.505 kcal/mol, was observed to form H-bonds with Met341 and Asp348. Comp83/Lovastatin (binding energy of-6.112 kcal/mol) formed H-bonds with Thr338. Comp96 (binding energy of-5.741 kcal/mol) formed H-bonds with Thr338, Ala390, and Asp404. Comp133 (binding energy of-7.774 kcal/mol) formed H-bonds with Met341, Asp348, and Asp404. Comp139/Kaempferol (binding energy of-8.475 kcal/mol) formed H-bonds Asp404 and Met341. Comp170/Pinocembrin (binding energy of-7.385 kcal/mol) formed H-bonds with Met341 and Asp404. Comp193/Drotaverine (binding energy of-4.923 kcal/mol) formed H-bonds with Asp404. Comp214 (binding energy of-9.209 kcal/mol) formed H-bonds with Met341, Asp404, and Asp348. Comp215/Salvigenin (binding energy of-8.624 kcal/mol) formed H-bonds with Met341 and exhibited pi-pi interaction with Lys295. Comp219/Hydroxyibuprofen (binding energy of-5.074 kcal/mol) formed H-bonds with Thr338 and Ser345 (**Figure S3**).

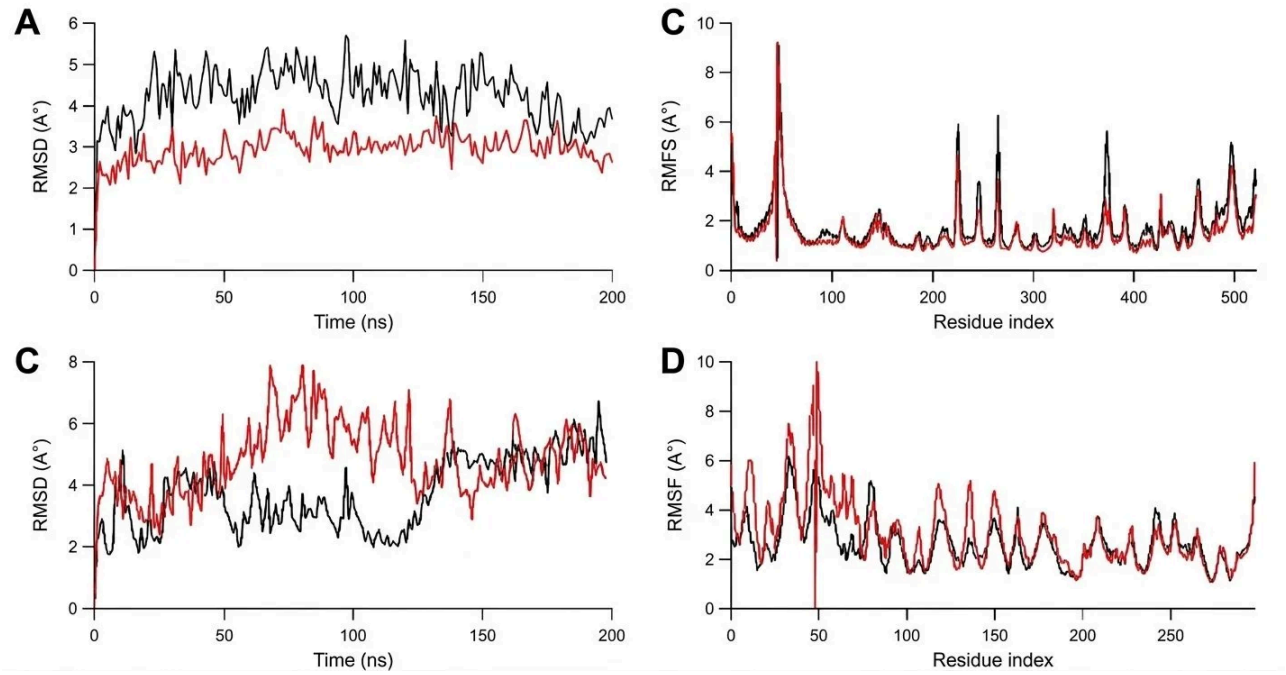


Figure 6. The RMSD and RMSF plots of the STAT3 and SRC systems. (A) RMSD and (B) RMSF plots of the STAT3 system bound to native ligand KQV (black) and Comp87/Picrocrocin (red). (C) RMSD and (D) RMSF plots of the SRC system bound to native ligand ANP (black) and Comp4 (red).

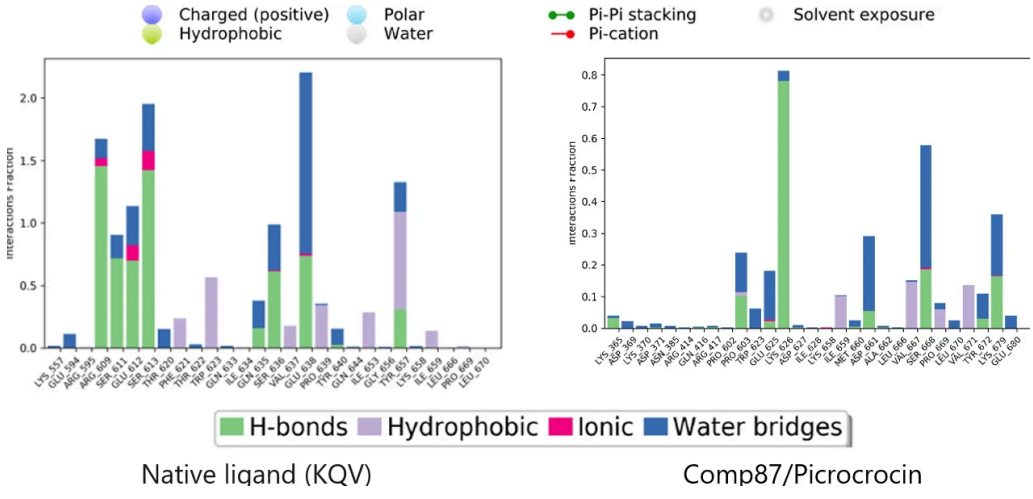


Figure 7. The 2D ligand–protein contacts of the ligands with STAT3 (PDB ID: 6NJS) and their respective protein–ligand contact histograms. Left: Native ligand (KQV) and right: Comp87/Picrocrocin.

Stability Assessment via Molecular Dynamics Simulations

The stability of the top protein-ligand complexes was evaluated through 200 ns molecular dynamics (MD) simulations. The Root Mean Square Deviation (RMSD) and Root Mean Square Fluctuation (RMSF) profiles indicated that the complexes generally reached equilibrium.

Molecular dynamics simulations with 200-ns timeframe were performed on STAT3 (PDB ID: 6NJS) with the native ligand (KQV) and Comp87/Picrocrocin. The STAT3-Comp87/Picrocrocin complex exhibited lower RMSD fluctuations in comparison to the native ligand (KQV) and a comparable RMSF with the native ligand, suggesting high stability (**Figure 6A** and **6B**).

The MDS performed on SRC (PDB ID: 2SRC) with the native ligand (ANP) and Comp4 showed that the SRC-Comp4 Complex demonstrated an RMSD similar to the native ligand (ANP), with a slightly higher RMSF, particularly in loop regions, while maintaining stable core interactions (**Figure 6C** and **6D**).

Protein–ligand contacts during the 200-ns MDS performed on STAT3 (PDB ID: 6NJS) demonstrated that KQV interacted through H-bonds with Arg609 (111% occupancy), Ser611 (71% occupancy), Glu612 (68% occupancy), Ser613 (70% occupancy), Ser636 (53% occupancy), and Glu638 (31% occupancy), and through a water-mediated H-bond with Glu638 (43% occupancy). On the other hand, Comp87/Picrocrocin exhibited an interaction through H-bonds with Lys626 (75% occupancy) (**Figure 7**).

Meanwhile, MDS conducted on SRC (PDB ID: 2SRC) revealed that ANP interacted through H-bond interaction with Leu273 (38% occupancy), Arg388 (45% occupancy), Arg385 (48% occupancy), and water-mediated H-bonds with Ala390 (38% occupancy), Phe278 (36% occupancy), Lys423 (41% occupancy), Asn391 (37% occupancy), and Lys295 (38% occupancy). Comp4 interacted through H-bond interaction with Asp348 (90% occupancy), Glu339 (62% occupancy), and Thr338 (64% occupancy) (**Figure 8**).

In summary, the ligands were able to maintain the interactions with the crucial residues of SRC during the 200-ns MDS, akin to the ligands that interacted with STAT3.

Discussion

The present *in silico* study nominates STAT3, IL6, and SRC as high-priority target candidates of the ethyl acetate fraction of *V. cofassus*, based on network-pharmacology profiling.

IL6 is a multifunctional cytokine that is consistently elevated in the serum and hepatic microenvironment of patients with chronic HCV infection (39). This elevation is not a passive bystander effect but an active contributor to disease progression, with higher IL6 levels correlating with increased liver inflammation, fibrosis, cirrhosis, and ultimately hepatocellular carcinoma (HCC) (40). Importantly, HCV core and NS5A proteins directly stimulate IL6 production, creating a positive feedback loop that sustains chronic inflammation and promotes a microenvironment conducive to viral persistence and hepatocarcinogenesis. Our identification of IL6 as a top hub protein thus aligns with its role as a master regulator of the hepatic inflammatory response to HCV.

STAT3 is the principal downstream transcriptional effector of IL6 signaling, and our findings position it at the nexus of the network. In the context of HCV, STAT3 is not merely a downstream bystander but is actively co-opted by the virus: HCV core protein directly interacts with and activates STAT3 via phosphorylation, while NS5A and NS4B proteins further promote STAT3 activation (41). Mechanistically, HCV infection induces reactive oxygen species, leading to activation of SRC and JAK2 kinases, which subsequently phosphorylate and activate STAT3. STAT3, a cytoplasmic transcription factor in the JAK-STAT pathway, is critically involved in the pathophysiology of liver disease (42). This pathway, essential for mediating cytokine and growth factor signals, contributes significantly to liver damage. Furthermore, STAT3 has been shown to promote the survival of cancer stem cells (CSCs), suggesting that targeting this pathway could be a viable therapeutic strategy (42).

On the other hand, the inhibition of the cellular protein SRC has emerged as a promising *host-targeted* therapeutic strategy for the treatment of hepatitis C. The significance of SRC stems from the fact that SRC is a key host factor that HCV exploits during multiple phases of its lifecycle. SRC, a non-receptor tyrosine kinase, is involved in several critical cellular signaling pathways. The hepatitis C

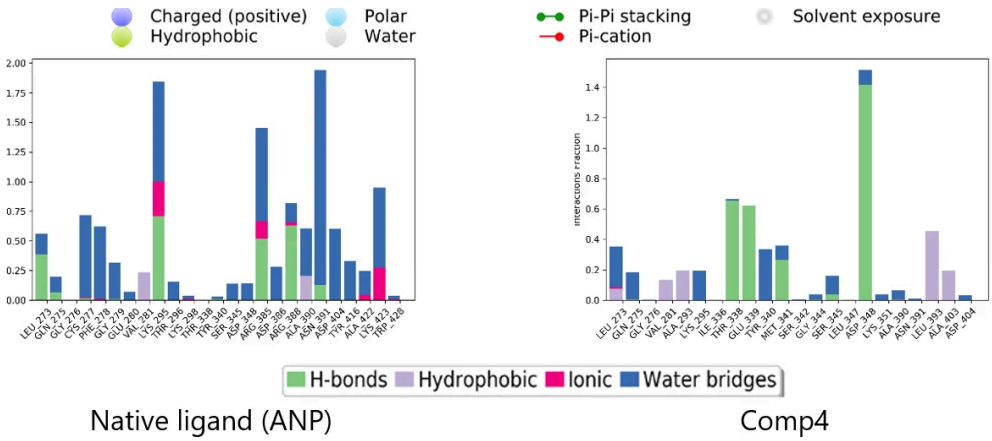


Figure 8. The 2D ligand–protein contacts of the ligands with SRC (PDB ID: 2SRC) and their respective protein–ligand contact histograms. Left: Native ligand (ANP) and right: Comp4.

virus (HCV) has co-opted these pathways for its own replication and survival. Inhibition of the SRC disrupts these viral hijacking mechanisms. The process by which HCV enters hepatocytes is a complex one, involving several host receptors. SRC kinase regulates the trafficking and function of key HCV entry receptors, particularly Claudin-1 (CLDN1) and Occludin (OCLN), to the cell surface. SRC inhibitors (e.g., Dasatinib, PP2) block the phosphorylation of these receptors, impairing their localization and function. This results in a significant decrease in the capacity of the HCV envelope glycoproteins to interact with the cell, consequently preventing viral entry (43). Furthermore, HCV replicates on a modified host membrane structure known as the "membranous web." SRC is involved in signal transduction pathways that are crucial for creating a favorable intracellular environment for viral replication. It can interact with and modulate the activity of other host factors that are required for the assembly of the viral replication complex. By blocking SRC, the formation and stability of the viral replication machinery are compromised. This leads to a significant reduction in the synthesis of new viral RNA (44).

In silico, the present study predicts that the Comp87/Picrocrocin–STAT3 bound complex exhibits inhibitory potential against STAT3. Concurrently, computational screening identifies Comp4, Comp20/Isorhamnetin, Comp25/4-Oxotretinoin, Comp49, Comp60, Comp72/Apigenin, Comp74/Padmatin, Comp83, Comp96, Comp133, Comp139/Kaempferol, Comp170/Pinocembrin, Comp193, Comp214, Comp215/Salvigenin, and Comp219 as putative SRC inhibitors.

Conclusion

The anti-hepatitis C potential of the ethyl acetate fraction of *V. cofassus* leaf was investigated using an integrated network pharmacology, molecular docking, and molecular dynamics simulations. A total of 201 common targets were identified between the plant's compounds and HCV-related genes, with STAT3, IL6, SRC, AKT1, EGFR, HSP90AA1, and TNF-α emerging as the most critical proteins. Functional enrichment analyses indicated that the predicted targets are involved in biological processes such as responses to chemicals and oxygen-containing compounds, intracellular signaling, stress, and the regulation of cell death programs, which were predominantly localized to junctions, vesicles, membrane domains, the cell surface, mitochondria, and the endoplasmic reticulum, while molecular functions are mainly linked to kinase and transferase activities, ATP binding, and protein-protein interactions. KEGG pathway mapping further linked these targets to a number disease pathways, including various cancers (e.g., prostate, Kaposi sarcoma), viral infections (e.g., hepatitis B, cytomegalovirus), and metabolic conditions such as atherosclerosis and diabetic complications. In the present study, Comp87/Picrocrocin showed predicted binding affinity for STAT3, while Comp4, Comp20/Isorhamnetin, Comp25/4-Oxotretinoin, Comp49, Comp60, Comp72/Apigenin, Comp74/Padmatin, Comp83, Comp96, Comp133, Comp139/Kaempferol, Comp170/Pinocembrin, Comp193, Comp214, Comp215/Salvigenin, and Comp219 were identified as potential SRC inhibitors based on docking scores. Molecular dynamics simulations further suggested stable binding of the compounds to key hepatitis C-related proteins, STAT3 and SRC under computational conditions. Consequently, the present *in silico* provides a computationally derived mechanistic hypothesis and identifies high-priority scaffolds for subsequent synthesis and testing which necessitate validation through *in vitro* and *in vivo* studies.

Declaration

Author Information

Puput Widarini, Master of Pharmacy, Faculty of Pharmacy, Universitas Halu Oleo, Kendari, 93232, Indonesia. **Contribution:** Investigation, Methodology.

Sri Wahyuli, Master of Pharmacy, Faculty of Pharmacy, Universitas Halu Oleo, Kendari, 93232, Indonesia. **Contribution:** Formal Analysis.

Ruslin Ruslin, Faculty of Pharmacy, Universitas Halu Oleo, Kendari, 93232, Indonesia. **Contribution:** Writing – Original Draft, Methodology.

Setyanto Tri Wahyudi, Department of Physics, Faculty of Mathematics and Natural Sciences, IPB University, Bogor, 16680, Indonesia. **Contribution:** Investigation, Methodology.

Muhammad Arba *(*Corresponding author)*, Faculty of Pharmacy, Universitas Halu Oleo, Kendari, 93232, Indonesia. **Contribution:** Conceptualization, Formal Analysis, Supervision, Validation.

Acknowledgment

During the preparation of this manuscript, the authors used ChatGPT-4 solely as an assistant for language editing, grammar correction, and improving readability. No data, figures, or original research concepts were generated using artificial intelligence. The authors thoroughly reviewed and edited all AI-assisted text, take full responsibility for the contents of the published article, and approved the final manuscript prior to submission.

Conflict of Interest

The authors declare no conflict of interest.

Data Availability

The datasets generated and/or analyzed during the current study are available from the corresponding author on reasonable request.

Ethics Statement

Not applicable.

Funding Information

The research was funded by Penelitian Tesis Magister grant of Ministry of Higher Education, Research, and Technology, Republic of Indonesia with contract number 068/C3/DT.05.00/PL/2025.

References

1. Yeung AWK, Heinrich M, Kijjoa A, Tzvetkov NT, Atanasov

AG. The ethnopharmacological literature: An analysis of the scientific landscape. Journal of Ethnopharmacology. 2020;250:112414. doi: https://doi.org/10.1016/j.jep.2019.112414

2. Souto EB, Durazzo A, Nazhand A, Lucarini M, Zaccardelli M, Souto SB, *et al*. *Vitex agnus-castus* L.: Main Features and Nutraceutical Perspectives. Forests. 2020;11(7):761. doi: https://doi.org/10.3390/f11070761

3. Rasyid FA, Fukuyoshi S, Ando H, Miyake K, Atsumi T, Fujie T, *et al*. A Novel Clerodane Diterpene from *Vitex cofassus*. Chem. Pharm. Bull. 2017;65(1):116-120. doi: https://doi.org/10.1248/cpb.c16-00775

4. Pan W, Liu K, Guan Y, Tan GT, Hung NV, Cuong NM, *et al*. Bioactive Compounds from *Vitex leptobotrys*. J. Nat. Prod. 2014;77(3):663-667. doi: https://doi.org/10.1021/np400779v

5. Ban Y, Xia T, Jing R, Guo Y, Geng Y, Ye Q, *et al*. *Vitex* Diterpenoids: Structural Diversity and Pharmacological Activity. Cpd. 2020;26(1):138-159. doi: https://doi.org/10.2174/1381612825666191216151703

6. Mottaghipisheh J, Kamali M, Doustimotlagh AH, Nowroozzadeh MH, Rasekh F, Hashempur MH, *et al*. A comprehensive review of ethnomedicinal approaches, phytochemical analysis, and pharmacological potential of *Vitex trifolia* L. Front. Pharmacol. 2024;15. doi: https://doi.org/10.3389/fphar.2024.1322083

7. Islam Z, Caldeira GI, Caniça M, Islam N, Silva O. *Vitex* Genus as a Source of Antimicrobial Agents. Plants. 2024;13(3):401. doi: https://doi.org/10.3390/plants13030401

8. Dogara AM, Al-Rawi SS, Hama HA. Traditional uses, bioactive compounds and pharmacological uses of *Vitex doniana* Sweet: A Review. Ethn Res Appl. 2025;30. doi: https://doi.org/10.32859/era.30.12.1-130

9. Singh A, Bharadvaja N. The therapeutic potential of *Vitex negundo*: a phytochemical exploration. Vegetos. 2025;39(2):464-479. doi: https://doi.org/10.1007/s42535-024-01127-4

10. Sirotkin AV. Effects, Mechanisms of Action and Application of *Vitex agnus-castus* for Improvement of Health and Female Reproduction. Phytotherapy Research. 2025;39(3):1484-1493. doi: https://doi.org/10.1002/ptr.8438

11. Husain SA, Perveen S, Khan MA, Parveen R, Insaf A, Parveen B, *et al*. An Updated Review on Traditional and Modern Aspects of *V. negundo*. Ctm. 2023;9(2):e270822208079. doi: https://doi.org/10.2174/2215083808666220827115915

12. Nyamweya B, Rukshala D, Fernando N, de Silva R, Premawansa S, Handunnetti S. Cardioprotective Effects of *V. negundo* : A Review of Bioactive Extracts and Compounds. J Evid Based Complementary Altern Med. 2023;28. doi: https://doi.org/10.1177/2515690x231176622

13. Devipriya S, Mohan P, Mohanan A, Vineeth PK. A Systematic Review on the Pharmacological Prospectives of *V. negundo* in Ayurveda Drug Research. Jnr. 2023:1153-1171. doi: https://doi.org/10.18311/jnr/2023/29806

14. Raekiansyah M, Ngwe Tun MM, Ang A, Lee A, Macalino SJ, Billones J, *et al*. Antiviral Activity of Medicinal Plant Extracts *V. negundo* and *Macaranga tanarius* Against *Sars-cov-2*-2. Pathogens. 2025;14(8):820. doi: https://doi.org/10.3390/pathogens14080820

15. Thomas E, Stewart LE, Darley BA, Pham AM, Esteban I, Panda SS. Plant-Based Natural Products and Extracts: Potential Source to Develop New Antiviral Drug Candidates. Molecules. 2021;26(20):6197. doi: https://doi.org/10.3390/molecules26206197

16. Tietjen I, Gatonye T, Ngwenya BN, Namushe A, Simonambanga S, Muzila M, *et al*. *Croton megalobotrys* Müll Arg. and *V. doniana* (Sweet): Traditional medicinal plants in a three-step treatment regimen that inhibit *in vitro* replication of HIV-1. Journal of Ethnopharmacology. 2016;191:331-340. doi: https://doi.org/10.1016/j.jep.2016.06.040

17. Kadir FA, Kassim NM, Abdulla MA, Yehye WA. Hepatoprotective Role of Ethanolic Extract of*Vitex negundo*in Thioacetamide-Induced Liver Fibrosis in Male Rats. Evidence-Based Complementary and Alternative Medicine. 2013;2013:1-9. doi: https://doi.org/10.1155/2013/739850

18. Ninfali P, Antonelli A, Magnani M, Scarpa ES. Antiviral Properties of Flavonoids and Delivery Strategies. Nutrients. 2020;12(9):2534. doi: https://doi.org/10.3390/nu12092534

19. Muhammad Arba, Sunandar Ihsan, Milba N. Mazida, Jamili Jamili, Tutik S. Wahyuni. Network Pharmacology-Based Prediction of the Mechanism of Anti-Hepatitis c virus of Kleinhovia Hospita L. Tropical Journal of Natural Product Research. 2025;9(9). doi: https://doi.org/10.26538/tjnpr/v9i9.46

20. Sumner LW, Lei Z, Nikolau BJ, Saito K, Roessner U, Trengove R. Proposed quantitative and alphanumeric metabolite identification metrics. Metabolomics. 2014;10(6):1047-1049. doi: https://doi.org/10.1007/s11306-014-0739-6

21. Daina A, Michielin O, Zoete V. SwissADME: a free web tool to evaluate pharmacokinetics, drug-likeness and medicinal chemistry friendliness of small molecules. Sci Rep. 2017;7(1). doi: https://doi.org/10.1038/srep42717

22. Daina A, Michielin O, Zoete V. SwissTargetPrediction: updated data and new features for efficient prediction of protein targets of small molecules. Nucleic Acids Research. 2019;47(W1):W357-W364. doi: https://doi.org/10.1093/nar/gkz382

23. Keiser MJ, Roth BL, Armbruster BN, Ernsberger P, Irwin JJ, Shoichet BK. Relating protein pharmacology by ligand chemistry. Nat Biotechnol. 2007;25(2):197-206. doi: https://doi.org/10.1038/nbt1284

24. Jiang LR, Qin Y, Nong JL, An H. Network pharmacology analysis of pharmacological mechanisms underlying the anti-type 2 diabetes mellitus effect of guava leaf. Arabian Journal of Chemistry. 2021;14(6):103143. doi: https://doi.org/10.1016/j.arabjc.2021.103143

25. Rebhan M, Chalifa-Caspi V, Prilusky J, Lancet D. GeneCards: a novel functional genomics compendium with automated data mining and query reformulation support. Bioinformatics. 1998;14(8):656-664. doi: https://doi.org/10.1093/bioinformatics/14.8.656

26. Amberger JS, Bocchini CA, Schiettecatte F, Scott AF, Hamosh A. OMIM.org: Online Mendelian Inheritance in Man (OMIM®), an online catalog of human genes and genetic disorders. Nucleic Acids Research. 2014;43(D1):D789-D798. doi: https://doi.org/10.1093/nar/gku1205

27. Shannon P, Markiel A, Ozier O, Baliga NS, Wang JT, Ramage D, *et al*. Cytoscape: A Software Environment for Integrated Models of Biomolecular Interaction Networks. Genome Res. 2003;13(11):2498-2504. doi: https://doi.org/10.1101/gr.1239303

28. Kanehisa M, Furumichi M, Tanabe M, Sato Y, Morishima K. KEGG: new perspectives on genomes, pathways, diseases and drugs. Nucleic Acids Res. 2016;45(D1):D353-D361. doi: https://doi.org/10.1093/nar/gkw1092

29. Letelier L, Gaete-Eastman C, Peñailillo P, Moya-León MA, Herrera R. Southern Species from the Biodiversity Hotspot of Central Chile: A Source of Color, Aroma, and Metabolites for Global Agriculture and Food Industry in a Scenario of Climate Change. Front. Plant Sci. 2020;11:1002. doi: https://doi.org/10.3389/fpls.2020.01002

30. Ge SX, Jung D, Yao R. ShinyGO: a graphical gene-set enrichment tool for animals and plants. Bioinformatics. 2019;36(8):2628-2629. doi: https://doi.org/10.1093/bioinformatics/btz931

31. Huang DW, Sherman BT, Lempicki RA. Systematic and integrative analysis of large gene lists using DAVID bioinformatics resources. Nat Protoc. 2008;4(1):44-57. doi: https://doi.org/10.1038/nprot.2008.211

32. Benjamini Y, Hochberg Y. Controlling the False Discovery Rate: A Practical and Powerful Approach to Multiple Testing. Journal of the Royal Statistical Society Series B: Statistical Methodology. 1995;57(1):289-300. doi: https://doi.org/10.1111/j.2517-6161.1995.tb02031.x

33. Darmin WOYPN, Arfan A, Ruslin R, Wu C, Arba M. Docking-Based Virtual Screening to Identify the Cysteine Protease Falcipain-2 Inhibitors of *Plasmodium falciparum*. molekul. 2024;19(3):406. doi: https://doi.org/10.20884/1.jm.2024.19.3.7376

34. Kumar V, Liu H, Wu C. Drug repurposing against *Sars-cov-2* receptor binding domain using ensemble-based virtual screening and molecular dynamics simulations. Computers in Biology and Medicine. 2021;135:104634. doi: https://doi.org/10.1016/j.compbiomed.2021.104634

35. Patel DC, Hausman KR, Arba M, Tran A, Lakernick PM, Wu C. Novel inhibitors to ADP ribose phosphatase of SARS-CoV-2 identified by structure-based high throughput virtual screening and molecular dynamics simulations. Comput Biol Med. 2022;140:105084. doi: https://doi.org/10.1016/j.compbiomed.2021.105084

36. Arba M, Paradis N, Wahyudi ST, Brunt DJ, Hausman KR, Lakernick PM, *et al*. Unraveling the binding mechanism of the active form of Remdesivir to RdRp of *Sars-cov-2* and designing new potential analogues: Insights from molecular dynamics simulations. Chemical Physics Letters. 2022;799:139638. doi: https://doi.org/10.1016/j.cplett.2022.139638

37. Arba M, Wahyudi ST, Brunt DJ, Paradis N, Wu C. Mechanistic insight on the remdesivir binding to RNA-Dependent RNA polymerase (RdRp) of *Sars-cov-2*. Computers in Biology and Medicine. 2021;129:104156. doi: https://doi.org/10.1016/j.compbiomed.2020.104156

38. Zhou W, Wang Y, Lu A, Zhang G. Systems Pharmacology in Small Molecular Drug Discovery. Ijms. 2016;17(2):246. doi: https://doi.org/10.3390/ijms17020246

39. Arba M, Ihsan S, Hatma FMI, Jamili J, Wahyudi ST, Wahyuni TS. Inhibition of Hepatitis C virus by *Avicennia marina* (Forssk.) Vierh. leaves extract: Liquid chromatography-high-resolution mass spectrometry, network pharmacology, molecular simulation, and *in vitro* study. J Herbmed Pharmacol. 2025;14(2):188-199. doi: https://doi.org/10.34172/jhp.2025.52905

40. Dai CY, Tsai YS, Chou WW, Liu T, Huang CF, Wang SC, *et al*. The IL-6/STAT3 pathway upregulates microRNA-125b expression in Hepatitis C virus infection. Oncotarget. 2018;9(13):11291-11302. doi: https://doi.org/10.18632/oncotarget.24129

41. Tsai CL, Chang JS, Yu MC, Lee CH, Chen TC, Chuang WY, *et al*. Functional Genomics Identifies Hepatitis-Induced STAT3–TYRO3–STAT3 Signaling as a Potential Therapeutic Target of Hepatoma. Clinical Cancer Research. 2020;26(5):1185-1197. doi: https://doi.org/10.1158/1078-0432.ccr-18-3531

42. Ali FE, Abdel-Reheim MA, Hassanein EH, Abd El-Aziz MK, Althagafy HS, Badran KS. Exploring the potential of drug repurposing for liver diseases: A comprehensive study. Life Sciences. 2024;347:122642. doi: https://doi.org/10.1016/j.lfs.2024.122642

43. Lupberger J, Zeisel MB, Xiao F, Thumann C, Fofana I, Zona L, *et al*. EGFR and EphA2 are host factors for Hepatitis C virus entry and possible targets for antiviral therapy. Nat Med. 2011;17(5):589-595. doi:

https://doi.org/10.1038/nm.2341

44. Rosnoblet C, Fritzinger B, Legrand D, Launay H, Wieruszeski JM, Lippens G, *et al*. Hepatitis C virus NS5B and Host Cyclophilin A Share a Common Binding Site on NS5A. Journal of Biological Chemistry. 2012;287(53):44249-44260. doi: https://doi.org/10.1074/jbc.m112.392209

Additional Information

How to Cite

Widarini P, Wahyuli S, Ruslin R, Wahyudi ST, Arba M. Unraveling the Anti-HCV Mechanism of the Ethyl Acetate Fraction of Vitex cofassus via Integrated Network Pharmacology and Molecular Dynamics Simulation. Sciences of Phytochemistry. 2026;5(2):346-358. https://doi.org/10.58920/sciphy0502687

Publisher Note

All claims expressed in this article are solely those of the authors and do not necessarily reflect the views of the publisher, editors, or reviewers. The publisher remains neutral regarding jurisdictional claims in published maps and institutional affiliations. Any product that may be evaluated in this article, or claim made by its manufacturer, is not guaranteed or endorsed by the publisher.

Open Access & Copyright

Copyright of the work remains with the authors (2026). This article is published under a Creative Commons Attribution 4.0 International License, permitting use, sharing, and adaptation with proper attribution.